Original Article

Institution of MECHANICAL ENGINEERS

Journal of ENGINEERING IN MEDICINE

Proc IMechE Part H:
J Engineering in Medicine
226(6) 441–449
© IMechE 2012
Reprints and permissions:
sagepub.co.uk/journalsPermissions.nav
DOI: 10.1177/0954411912443207
pih.sagepub.com
SAGE

# Macroscopic and microscopic observations of needle insertion into gels

**Youri RJ van Veen, Alex Jahya and Sarthak Misra**

**Abstract**

Needle insertion into soft tissue is one of the most common medical interventions. This study provides macroscopic and microscopic observations of needle–gel interactions. A gelatin mixture is used as a soft-tissue simulant. For the macroscopic studies, system parameters, such as insertion velocity, needle diameter, gel elasticity, needle tip shape (including bevel angle) and insertion motion profile, are varied, while the maximum insertion force and maximum needle deflection are recorded. The needle tip and gel interactions are observed using confocal microscopic images. Observations indicate that increasing the insertion velocity and needle diameter results in larger insertion forces and smaller needle deflections. Varying the needle bevel angle from 8° to 82° results in the insertion force increasing monotonically, while the needle deflection does not. These variations are due to the coupling between gel rupture and tip compression interactions, which are observed during microscopic studies. Increasing the gel elasticity results in larger insertion forces and needle deflections. Varying the tip shapes demonstrates that bevel-tipped needles produce the largest deflection, but insertion force does not vary among the tested tip shapes. Insertion with different motion profiles are performed. Results show that adding 1 Hz rotational motion during linear insertion decreases the needle deflection. Increasing the rotational motion from 1 Hz to 5 Hz decreases the insertion force, while the needle deflection remains the same. A high-velocity (250 mm/s and 300 mm/s) tapping during insertion yields no significant decrease in needle deflection and a slight increase in insertion force.

**Keywords**

Bevel-tip needle, biopsy, confocal microscopy, elasticity, needle insertion, needle–tissue interactions, tissue rupture

Date received: 15 November 2011; accepted: 5 March 2012

## Introduction

Percutaneous needle insertion is one of the most common minimally invasive medical interventions used for diagnosis (e.g. biopsy) and drug delivery (e.g. brachytherapy). Accurate needle placement in these procedures is of utmost importance because biopsy of an unintended tissue region can result in misdiagnosis, or, in the case of brachytherapy, malignant tissue is not destroyed. Inaccuracy during needle placement can be caused by several factors, such as tissue inhomogeneity and anisotropy, anatomical obstructions, and physiological processes like fluid flow and respiration. Such targeting errors can be reduced by using a robot to insert and steer the needle towards the target. Several research groups have investigated the use of robotic needle insertion devices.[1–10] In order to control and accurately steer the needle, the interaction dynamics between the needle and tissue needs to be understood.

Several parameters that affect needle and tissue interaction have been identified by the previously mentioned researchers. There parameters include needle insertion velocity and motion profile, needle geometric properties, such as diameter, tip shape and bevel angle, and tissue elastic properties. Macroscopic observations have been carried out to study the effect of these parameters on needle deflection, target motion and interaction forces. Kataoka et al.[11] studied the interaction forces at the tip and along the shaft of a triangular-pyramid-tipped needle during insertion into canine prostate. Okamura et al.[12] reported that needles with an

MIRA–Institute for Biomedical Technology and Technical Medicine, University of Twente, The Netherlands

**Corresponding author:**
Youri RJ van Veen, MIRA–Institute for Biomedical Technology and Technical Medicine, University of Twente, Enschede, The Netherlands.
Email: y.r.j.vanveen@utwente.nl

asymmetric tip (e.g. bevel tip) have a large deflection and thus would be suitable for steering. Podder et al.[13] studied the effect of different insertion velocities (both linear and angular) on interaction forces and target motion. They used a diamond-tip-shaped needle, but did not investigate needle deflection. Lagerburg et al.[3] demonstrated that high-velocity tapping during needle insertion reduced prostate motion. Abolhassani et al.[14] studied different insertion methods using bevel-tipped needles. They reported that needle rotation during linear insertion decreases needle deflection.

This study presents the effects of the above-mentioned system parameters on insertion forces and needle deflection. These include both macroscopic and microscopic observations. Confocal microscopic studies investigate the interactions occurring at the needle tip. The phenomenon observed in the macroscopic and microscopic studies are linked.

## Experimental setup

### *Macroscopic observations*

A two degree-of-freedom (DOF) needle insertion device (Figure 1) is designed for the macroscopic observations. The device permits translation along and rotation about the *z*-axis. It consists of a Misumi translation (type LX3010) stage (MISUMI Group Inc. Tokyo, Japan) actuated with a Maxon motor (type RE25, with GP26B gearhead, transmission ratio 4.4:1), and the rotational motion is accomplished by using a Maxon Motor (type ECMax22) (MaxonMotor, Sachseln, Switzerland). Two Elmo Whistle 2.5/60 controllers (Elmo Motion Control Ltd, Petach-Tikva, Israel) are used to control the motors.

Needle and soft-tissue simulant interaction forces and torques are measured using a six-axis Nano17 force/torque sensor (ATI Industrial Automation, Apex, USA) mounted at the needle base. The force and torque resolution of the sensor are 3.1 mN and 15.6 mN-mm, respectively. Moreover, needle insertion is recorded at 30 frames/s via a Sony XCD-SX90 charge-coupled device FireWire camera (Sony Corporation, Tokyo, Japan) placed 450 mm above the insertion (*yz*)-plane. A tracking algorithm is used to capture the needle tip position from the recorded images.[15]

All experiments are performed on soft-tissue simulants made from a gelatin mixture. The gels consist of 8%, 14.9% and 20% mass percentage of gelatin-to-water mixture, which results in an elasticity of $E_1 = 8.7$ kPa, $E_2 = 35.5$ kPa and $E_3 = 58.1$ kPa, respectively. Needles are made from solid stainless steel wires. The parameters that are investigated include insertion velocity, bevel angle, needle diameter, gel elasticity, motion profile and needle tip shape (Figure 2). The six sets of experimental studies are tabulated in Table 1.

### *Microscopic observations*

Microscopic observations of needle–gel interactions at the needle tip is carried out using a single DOF insertion device and a Zeiss Laser Scanning Confocal Microscope (LSCM) 510 microscope (Figure 3). The imaging plane is *xz*, while needle insertion is along the *z*-axis. The interactions are visualized with differential interference contrast (DIC), epifluorescence using the 488 Nm line of the argon laser and a 10× objective lens. In order to facilitate epifluorescent imaging, the gel is doped with fluorescein isothiocyanate. Gel rupture and tip compression are visualized using DIC and epifluorescent images.

The needle–gel interaction forces and torques are measured using the Nano17 force/torque sensor. Solid stainless steel needles of diameter 1 mm and 1.6 mm, and bevel angles 30°, 60° and 75° are used in the experiments. The needles are inserted at two velocities (0.5 mm/s and 1 mm/s) for a distance of 7 mm.

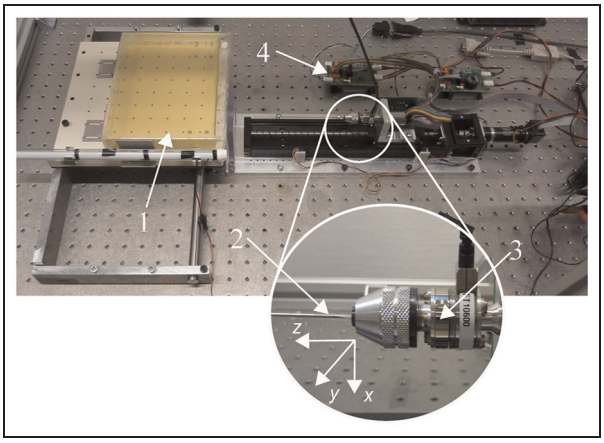


**Figure 1.** Two degree-of-freedom needle insertion setup used for the macroscopic observations. 1: Gelatin block; 2: needle; 3: force/torque sensor; 4: controllers. Insertion is along the z-axis, and the needle is oriented such that deflection is predominantly in the *yz*-plane.

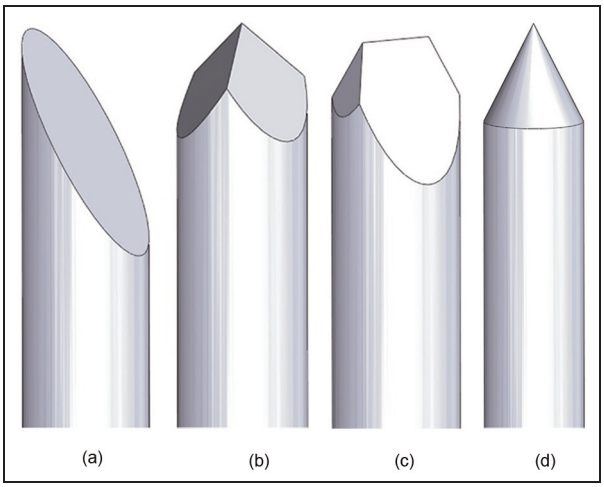


**Figure 2.** Various needle tip shapes used in the experiments: (a) bevel, (b) franseen, (c) diamond, (d) conical.

**Table 1.** Experimental plan for macroscopic observations. v: Insertion velocity; $\phi$: needle diameter; $\beta$: bevel angle; E: gel elasticity, where $E_1 = 8.7$ kPa, $E_2 = 35.5$ kPa and $E_3 = 58.1$ kPa. Tip shape: bevel, franseen, diamond and conical. Motion profile: continuous, rotation and tapping motions. Continuous linear insertion is performed at 10 mm/s. Rotational motion is a sinusoidal motion profile of frequency 1 Hz, 2.5 Hz and 5 Hz, combined with continuous linear insertion. Angular displacement of 180° is used. Tapping motion involves inserting the needle in steps of 20 mm with an insertion velocity of 250 mm/s and 300 mm/s. The needle insertion distance is 100 mm for all experiments. Each experiment is repeated three times.

| System parameters | | | | | | | | | | | | | | | | | | | | | | | | | | | | | | | | |
|---|---|---|---|---|---|---|---|---|---|---|---|---|---|---|---|---|---|---|---|---|---|---|---|---|---|---|---|---|---|---|---|---|
| Experiment | v (mm/s) | | | | | | | | $\phi$ (mm) | | | $\beta$ (o) | | | | | | E (kPa) | | | Tip shape | | | | Motion profile | | | | | | |
| | 5 | 10 | 20 | 50 | 100 | 150 | 200 | 250 | 300 | 1 | 1.6 | 2 | 8 | 15 | 30 | 45 | 55 | 65 | 75 | 82 | $E_1$ | $E_2$ | $E_3$ | Bevel | Franseen | Diamond | Conical | Continuous | Rotation | | Tapping |
| | | | | | | | | | | | | | | | | | | | | | | | | | | | | | 1 Hz | 2.5 Hz | 5 Hz | |
| #1 | | ✓ | ✓ | ✓ | ✓ | ✓ | ✓ | ✓ | ✓ | ✓ | | | | ✓ | ✓ | | | | | | | ✓ | | ✓ | | | | ✓ | | | | |
| #2 | | | ✓ | | | | | | | ✓ | ✓ | ✓ | | | ✓ | | | | | | | ✓ | | ✓ | | | | ✓ | | | | |
| #3 | | | ✓ | | | | | | | ✓ | ✓ | ✓ | | | ✓ | | | | | | ✓ | | ✓ | ✓ | | | | ✓ | | | | |
| #4 | | | ✓ | | | | | | | ✓ | | | ✓ | ✓ | ✓ | ✓ | ✓ | ✓ | ✓ | ✓ | | ✓ | ✓ | ✓ | | | | ✓ | | | | |
| #5 | | | ✓ | | | | | | | ✓ | | | | | ✓ | | | | | | | | | | ✓ | | ✓ | ✓ | | | | |
| #6 | | | ✓ | | | | | | | ✓ | | | | | ✓ | | | | | | | ✓ | | ✓ | | | | ✓ | | ✓ | ✓ | ✓ |

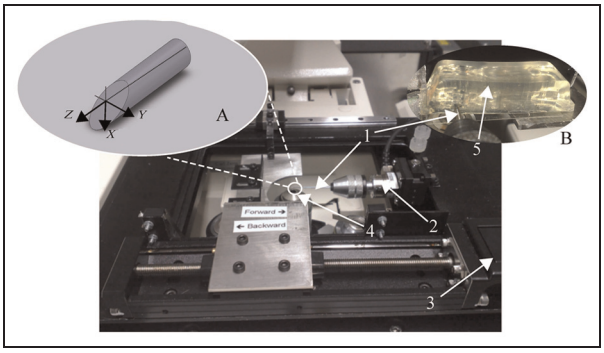


**Figure 3.** Experimental setup for the microscopic observations. The needle–gel interaction is observed using a laser scanning confocal microscope (inset A shows the needle tip with bevel angle of 45°, while inset B shows the needle insertion into a gelatin block). 1: needle; 2: force/torque sensor; 3: linear stage; 4: microscope objective lens; 5: gelatin block. The imaging plane is *xz*, the insertion direction is along the *z*-axis and the in-plane bending torque is about the *y*-axis.

## Results

In this section, observations of the macroscopic and microscopic studies are presented. Experimental results include force and torque data, needle tip deflection and microscopic images of needle–gel interactions.

### *Macroscopic observations*

Three insertions are performed for each experiment provided in Table 1. The average of the three data points are presented in the results below. The percentage changes in the maximum insertion force ($|F_{z,\max}|$) and maximum needle deflection ($|\delta_{\max}|$) are calculated as

$$\left(\frac{|F_{z,\max}^{\text{final}}| - |F_{z,\max}^{\text{initial}}|}{|F_{z,\max}^{\text{initial}}|} \times 100\right)$$

and

$$\left(\frac{|\delta_{\max}^{\text{final}}| - |\delta_{\max}^{\text{initial}}|}{|\delta_{\max}^{\text{initial}}|} \times 100\right)$$

respectively. In the above equations, $|F_{z,\max}^{\text{initial}}|$, $|F_{z,\max}^{\text{final}}|$ and $|\delta_{\max}^{\text{initial}}|$, $|\delta_{\max}^{\text{final}}|$ are the initial and final maximum insertion forces and maximum needle deflections, respectively.

*Experiment #1 (variation in insertion velocity).* $|F_{z,\max}|$ increases by 226% as insertion velocity (v) increases from 5 mm/s to 300 mm/s (Figure 4(a)). For the same variation in insertion velocity, $|\delta_{\max}|$ decreases by 10%. Moreover, the increase in $|F_{z,\max}|$ and decrease in $|\delta_{\max}|$ is less at higher insertion velocities. Average standard deviations in $|F_{z,\max}|$ and $|\delta_{\max}|$ are 0.08 N and 0.18 mm, respectively.

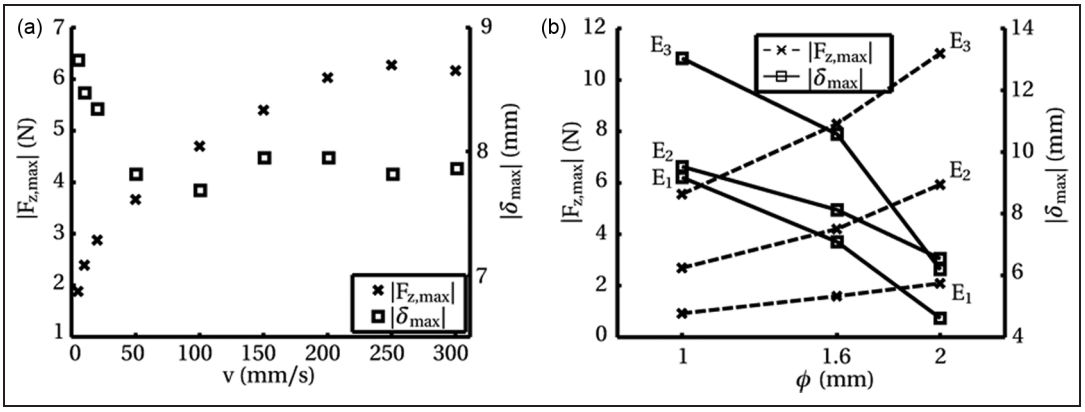


**Figure 4.** Maximum insertion force ($|F_{z,max}|$) and maximum needle tip deflection ($|\delta_{max}|$) for variation in: (a) insertion velocity (v) and (b) needle diameter ($\phi$) and gel elasticity ($E_1$=8.7 kPa, $E_2$=35.5 kPa and $E_3$=58.1 kPa). For (a), $E_2$=35.5 kPa, $\phi$= 1 mm and $\beta$ = 30°, while for (b), v=10 mm/s and $\beta$ = 30. Average standard deviations in (a) for $|F_{z,max}|$ and $|\delta_{max}|$ are 0.08 N and 0.18 mm, respectively. Average standard deviations in (b) for $|F_{z,max}|$ and $|\delta_{max}|$ are 0.22 N and 0.39 mm, respectively.

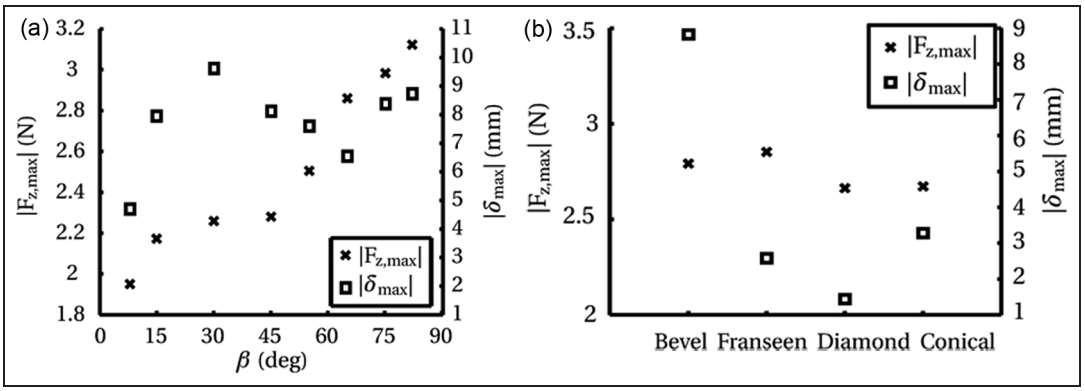


**Figure 5.** Maximum insertion force $|F_{z,max}|$ and maximum needle tip deflection $|\delta_{max}|$ for variation in: (a) bevel angle ($\beta$) and (b) tip shape. In both experiments, $E_2$=35.5 kPa, v=10 mm/s and $\phi$ = 1 mm. Average standard deviations in (a) for $|F_{z,max}|$ and $|\delta_{max}|$ are 0.08 N and 0.15 mm, respectively. Average standard deviations in (b) for $|F_{z,max}|$ and $|\delta_{max}|$ are 0.14 N and 0.18 mm, respectively.

*Experiment #2 (variation in needle diameter).* Increase in the needle diameter ($\phi$) from 1 mm to 2 mm results in a 126%, 120% and 98% increase in $|F_{z,max}|$ for gel elasticity, $E_1$, $E_2$ and $E_3$, respectively (Figure 4(b)). For the same variation in $\phi$ and $E_1$, $E_2$ and $E_3$, $|\delta_{max}|$ decreases by 50%, 31% and 52%, respectively. For larger diameter needles, the second moment of inertia ($I_{needle}$) increases $\left(I_{needle} = \frac{\pi\phi^4}{64}\right)$, which results in less needle deflection. Average standard deviations in $|F_{z,max}|$ and $|\delta_{max}|$ are 0.22 N and 0.39 mm, respectively.

*Experiment #3 (variation in gel elasticity).* Increase in the gel elasticity from $E_1$ to $E_3$ causes $|F_{z,max}|$ to increase by 502%, 420% and 427% for $\phi$ being 1 mm, 1.6 mm and 2 mm, respectively (Figure 4(b)). Furthermore, for the same variation in gel elasticity, $|\delta_{max}|$ increases by 40%, 49% and 34% for $\phi$ being 1 mm, 1.6 mm and 2 mm, respectively.

*Experiment #4 (variation in needle tip bevel angle).* Variation in bevel angle ($\beta$) results in $|F_{z,max}|$ increasing monotonically, while $|\delta_{max}|$ does not (Figure 5(a)). For $\beta$ varying from 8° to 82°, $|F_{z,max}|$ increases by 59%. Increase in $\beta$ from 8° to 30° causes $|\delta_{max}|$ to increase by 104%. However, a further increase in $\beta$ to 65° results in a 32% drop in $|\delta_{max}|$. The trend reverses back to a 34% increase in $|\delta_{max}|$ as $\beta$ increases from 65° to 82°. This non-monotonic relationship for $|\delta_{max}|$ is explained below using microscopic observations. Average standard deviations in $|F_{z,max}|$ and $|\delta_{max}|$ are 0.08 N and 0.15 mm, respectively.

*Experiment #5 (variation in tip shapes).* Results indicate that $|F_{z,max}|$ is relatively constant (~2.8 N) for all needle tip shapes (Figure 5(b)). The bevel-tipped needle is observed to have the largest $|\delta_{max}|$ (8.8 mm). This is due to the asymmetric force distribution at the bevel tip. Variation in deflection for needles with symmetric tips, such as franseen, diamond or conical, is observed to be minimal. Small deflection is noted for the needles with symmetric tips due to needle bending prior to insertion. Average standard deviations in $|F_{z,max}|$ and $|\delta_{max}|$ are 0.14 N and 0.18 mm, respectively.

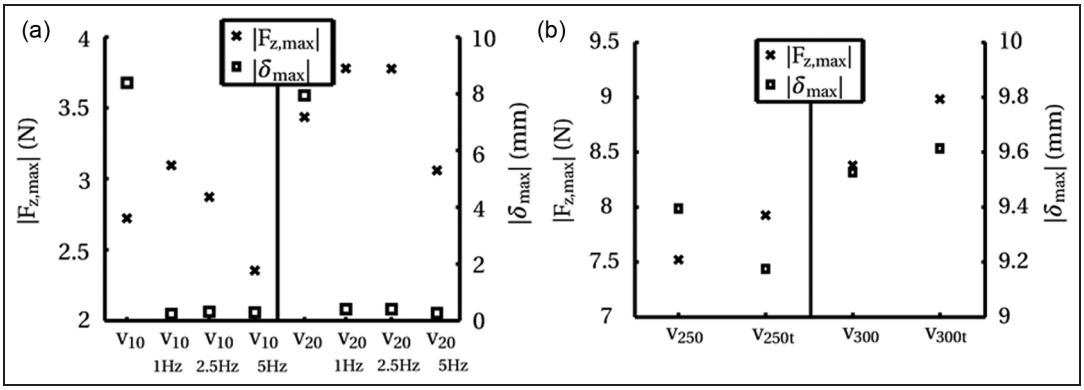


**Figure 6.** Maximum insertion force ($|F_{z,max}|$) and maximum needle tip deflection ($|\delta_{max}|$) for: (a) continuous linear insertion with rotation and (b) tapping motion. In both experiments, $E_2$=35.5 kPa, $\phi$= 1 mm and $\beta$ = 30°. For (a), the motion profiles are: v=10 mm/s and v=20 mm/s without and with rotation (1 Hz, 2.5 Hz and 5 Hz). For (b), the motion profiles are: v = 250 mm/s and v = 300 mm/s without and with tapping motion (subscript t). Tapping motion involves needle insertion in steps of 20 mm with a pause of 500 ms between each step. Average standard deviations in (a) for $|F_{z,max}|$ and $|\delta_{max}|$ are 0.02 N and 0.18 mm, respectively. Average standard deviations in (b) for $|F_{z,max}|$ and $|\delta_{max}|$ are 0.25 N and 0.18 mm, respectively.

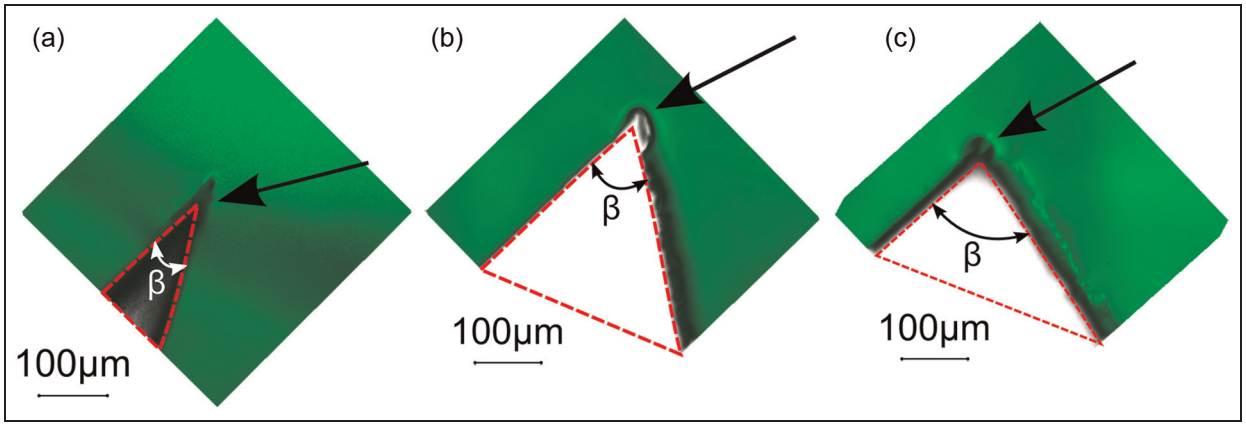


**Figure 7.** Epifluorescent images of gel rupture (shown with an arrow) for variation in bevel angle ($\beta$): (a) 30°, (b) 60° and (c) 75°. Rupture is observed to be longest and narrowest for $\beta$ = 30°, while it is shortest and widest for $\beta$ = 75°.

*Experiment #6 (variation in motion profiles).* Figure 6(a) shows that the addition of 1 Hz rotational motion to the continuous linear insertion of v = 10 mm/s and v = 20 mm/s results in 97% and 96% decreases in $|\delta_{max}|$, respectively. Furthermore, addition of 1 Hz rotational motion for v = 10 mm/s and v = 20 mm/s results in 14% and 10% increases in $|F_{z,max}|$, respectively. Increasing the rotational motion to 5 Hz results in decreases in $|F_{z,max}|$ by 24% and 19%, for v = 10 mm/s and v = 20 mm/s, respectively. However, no significant effect is observed for $|\delta_{max}|$. Average standard deviations in $|F_{z,max}|$ and $|\delta_{max}|$ are 0.02 N and 0.18 mm, respectively.

The effect of tapping motion on needle deflection and insertion force is shown in Figure 6(b). Results show that tapping motion increases $|F_{z,max}|$ by 5% and 7% for v = 250 mm/s and v = 300 mm/s, respectively. Yet, no significant effect is noted for $|\delta_{max}|$ (~ 0.2 mm). Average standard deviations in $|F_{z,max}|$ and $|\delta_{max}|$ are 0.25 N and 0.18 mm, respectively.

## Microscopic observations

Microscopic observations are performed to investigate the interactions at the needle tip and their effects on deflection. Needle insertions are conducted at 0.5 mm/s and 1 mm/s due to limitations with the confocal microscopic image-scanning rate (approximately 2 s/scan). The experimental results indicate the presence of gel rupture and compression occurring at the needle tip, as shown in Figures 7 and 8, respectively. Note, the results presented in Figures 9 to 12 are from a single representative experiment. Each experimental case is performed three times, and trends are the same in all cases.

Gel rupture is observed to be narrow and long for a small bevel angle ($\beta$ = 30°), and becomes wider and shorter for a large bevel angle ($\beta$ = 75°). A needle with a large bevel angle has a blunter tip, resulting in less gel rupture during insertion (Figure 7). Furthermore, larger bevel angles result in increased gel compression (Figure 8). Microscopic observations are reported for

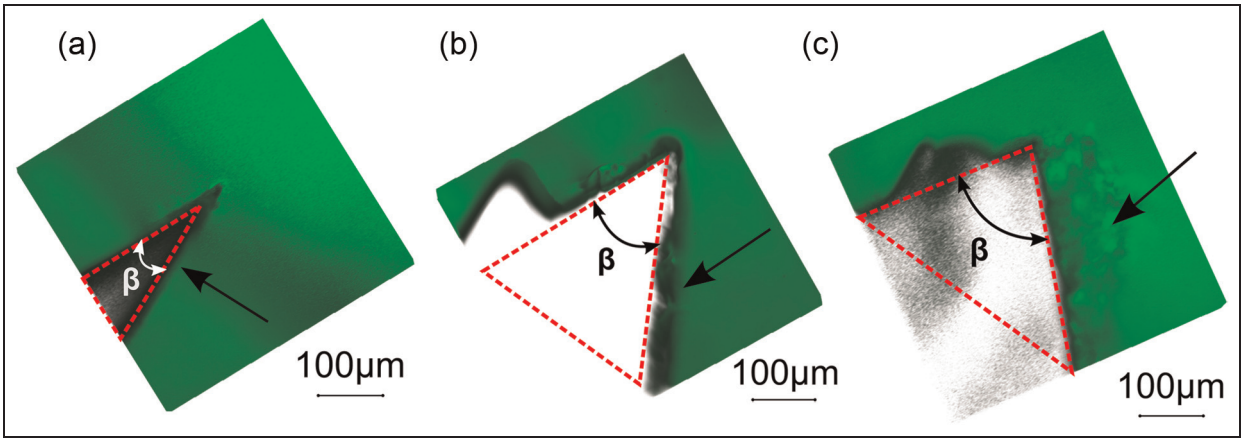


**Figure 8.** Epifluorescent images of gel compression (shown with an arrow) for variation in bevel angle ($\beta$): (a) 30°, (b) 60° and (c) 75°. Compression is observed to be most for $\beta = 75°$.

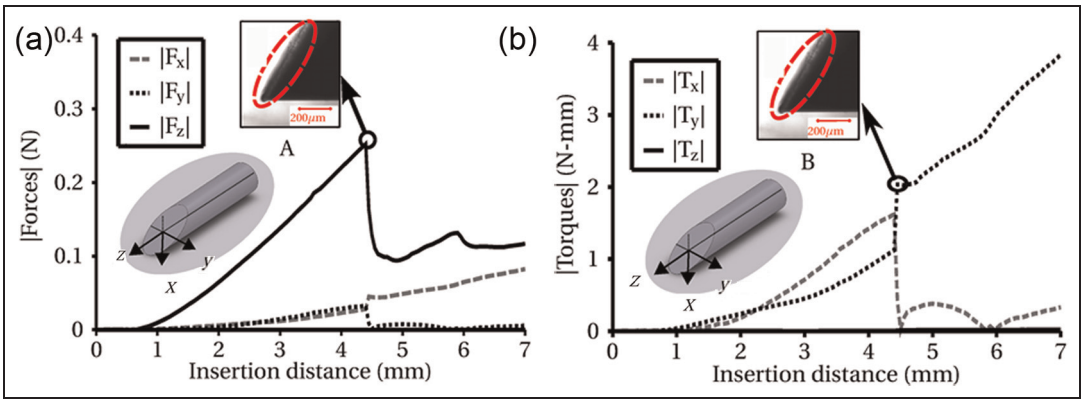


**Figure 9.** Needle–gel interaction forces and torques. Gel rupture results in a sudden drop in insertion force ($|F_z|$) and torque about the $x$-axis ($|T_x|$). The needle diameter ($\phi$) and bevel angle ($\beta$) are 1 mm and 60°, respectively. The needle is inserted at v=0.5 mm/s into a gel of elasticity $E_2 = 35.5$ kPa. The opening created due to gel rupture is marked in red. This opening provides space for the needle to bend, and the in-plane bending torque ($|T_y|$) increases after rupture. In (b), $|T_z|$ is zero.

large bevel angles ranging from 30°–75°, since gel rupture and tip compression are visible for these angles. Nevertheless, our hypothesis can be extended to small bevel angles (5°–15°). For these angles, gel rupture is the most dominant factor.

The needle–gel interaction forces and torques are shown in Figure 9. Gel rupture is characterized by a sudden drop in the insertion force ($|F_z|$). Rupture creates an opening at the needle tip and is depicted in the DIC images (Figure 9). This causes a drop in $|F_z|$, and provides space for the needle to bend in the $xz$-plane. The needle tip bending torque in the plane of insertion is $|T_y|$, and $|T_y|$ increases as rupture occurs. The process of gel rupture and tip compression continues to occur as the needle traverses through the gel, and $|F_z|$ and $|T_y|$ progressively increase.

Tip compression increases for a larger bevel angle ($\beta = 75°$), which results in an increase in $|F_z|$ (Figure 10(a)). Gel rupture is the shortest and widest for $\beta = 75°$, which results in the most significant decrease in $|F_z|$ and increase in $|T_y|$, as compared to the other bevel angles (Figure 10). This significant increase in $|T_y|$ for $\beta = 75°$, as compared to $\beta = 60°$, results in a larger needle deflection (Figure 5(a)).

Increase in the needle diameter, for constant bevel angles and insertion velocities, results in larger interaction surface areas at the bevel edge. Hence, $|F_z|$ increases for larger diameter needles (Figure 11). The increase in the needle diameter results in greater resistance to bending (increase in the second moment of inertia). This resistance is more significant than the in-plane needle tip bending torque ($|T_y|$). Thus, even though $|T_y|$ increases, the needle deflection decreases as the needle diameter increases (Figure 4(b)). Results consistent to the 1 mm/s insertion velocity are also observed for 0.5 mm/s. Furthermore, for softer gels, $|F_z|$ and $|T_y|$ are lower (Figure 12), which results in a smaller needle deflection. This hypothesis is consistent with the macroscopic observations shown in Figure 4(b).

## Discussion

This study presents both macroscopic and microscopic observations of needle–gel interactions. Experiments

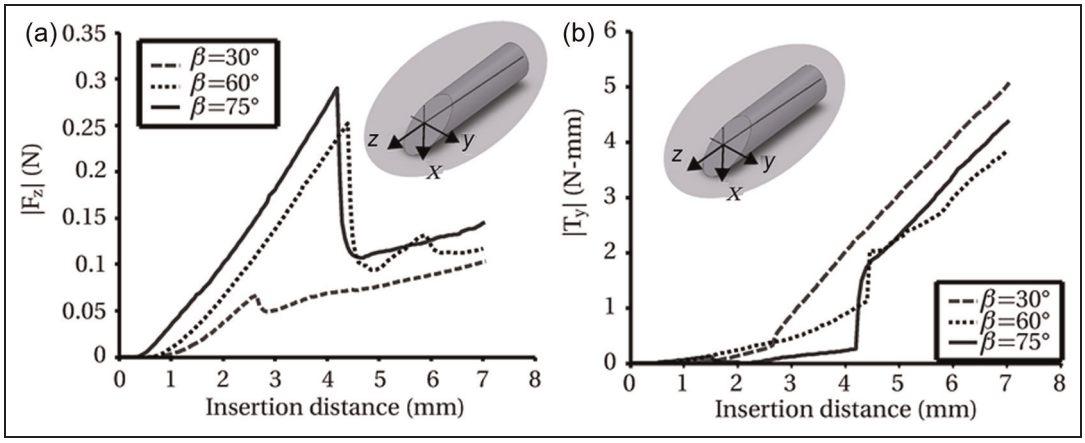


**Figure 10.** Variation in insertion force $(|F_z|)$ and in-plane bending torque $(|T_y|)$ for change in bevel angle $(\beta)$. The needle diameter $(\phi)$ is 1 mm. The needle is inserted at v = 0.5 mm/s into a gel of elasticity $E_2$ = 35.5 kPa..

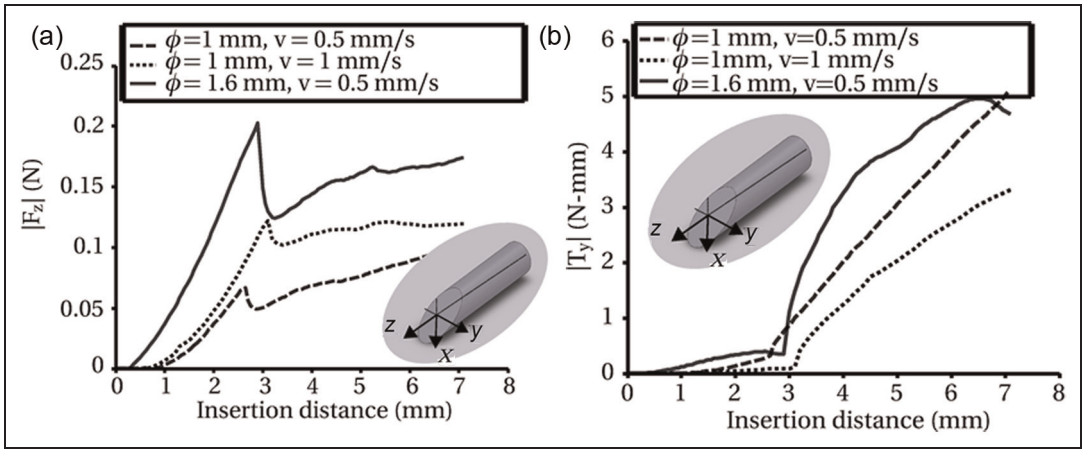


**Figure 11.** Variation in insertion force $(|F_z|)$ and in-plane bending torque $(|T_y|)$ for changes in needle diameter $(\phi)$ and insertion velocity (v). The bevel angle $(\beta)$ is 30°. The needle is inserted into the gel of elasticity $E_2$ = 35.5 kPa.

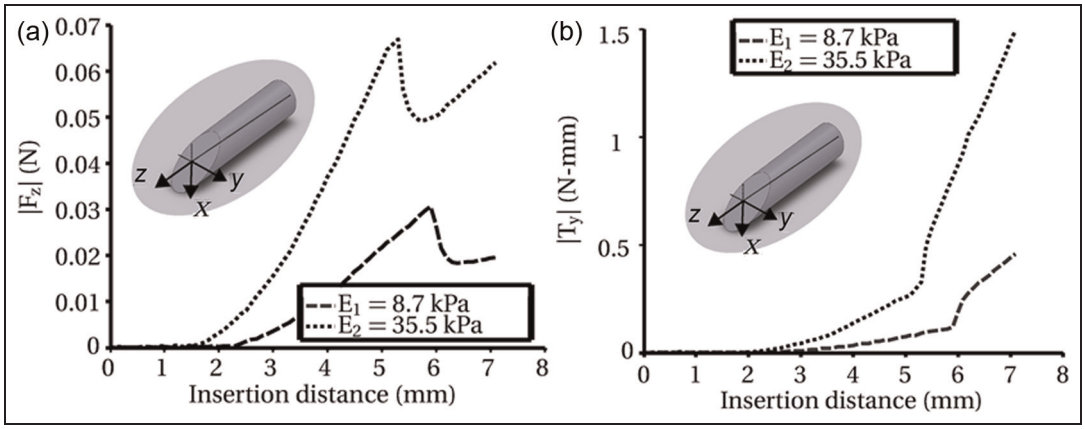


**Figure 12.** Variation in insertion force $(|F_z|)$ and in-plane bending torque $(|T_y|)$ for change in gel elasticity ($E_1$ and $E_2$). The needle diameter $(\phi)$ and bevel angle $(\beta)$ are 1 mm and 60°, respectively. The needle is inserted at v = 0.5 mm/s.

are conducted where the insertion velocity, needle diameter, bevel angle, gel elasticity, needle tip shape and motion profile are varied. Increasing the needle insertion velocity (from 5 mm/s to 300 mm/s) results in the maximum insertion force asymptotically increasing, and the maximum needle deflection asymptotically

decreasing. Increasing the needle diameter (from 1 mm to 2 mm) results in a decrease in the deflection, but an increase in the insertion force. The second moment of inertia of the needle increases for larger diameter, which results in greater resistance to needle bending. This explains the diminished deflection of the needle.

Varying the bevel angle results in the maximum insertion force increasing monotonically. During needle insertion, microscopic observations indicate the occurrence of both rupture and compression of the gel at the tip. For a needle with a small bevel angle ($\beta = 30°$), there is less compression of the gel as compared to a needle with a large bevel angle ($\beta = 75°$). More compression of the gel results in higher insertion forces. For $\beta = 75°$, gel rupture is wide and short, while for $\beta = 30°$, gel rupture is narrow and long. For a large bevel angle ($\beta = 75°$), coupling of high insertion force, and wide and short gel rupture results in more deflection compared to a needle with $\beta = 60°$. Furthermore, for a small bevel angle ($\beta = 30°$), coupling of low insertion force, and long and narrow gel rupture also results in more deflection compared to a needle with $\beta = 60°$. These microscopic observations explain the non-monotonic variation in the maximum needle deflection. In general, increasing the gel elasticity from $E_1 = 8.7$ kPa to $E_3 = 58.1$ kPa results in larger insertion forces and needle deflections.

Four different needle tip shapes are investigated, and a bevel-tipped needle is found to result in the largest needle deflection due to its asymmetric shape. However, insertion force does not vary significantly among the tested tip shapes. Different motion profiles are also investigated. Results show that adding 1 Hz sinusoidal rotation during linear insertion with a bevel-tipped needle decreases the amount of needle deflection, but increases the insertion force, which could indicate more tissue damage. Increasing the rotational motion decreases the insertion force, which could indicate less tissue damage. A high-velocity tapping motion during insertion does not result in significant changes in needle deflection, but it does increase the insertion force. However, this method could still be used in medical interventions since it does result in reduced organ motion.[3]

From the presented results, it can be concluded that friction forces are an integral part of the needle–tissue interaction forces. Their effects on needle deflection also need to be studied. In addition to understanding the needle–tissue interaction forces, these studies would also help quantify tissue damage. Microscopic studies of needle–tissue interaction could aid in quantifying tissue damage, as well as modelling of the rupture effect.[16] An immediate extension to this study could be the inclusion of biopsy needles. Furthermore, out-of-plane needle deflection could be measured by incorporating three-dimensional tracking of the needle tip. A preliminary set of experiments were conducted to measure in- and out-of-plane needle deflection during insertion in homogeneous gel and soft biological tissue. Results from these experiments show similar trends with respect to in-plane needle deflection presented in the current study. Depending on the organ, biological tissue varies in homogeneity and elasticity. Nonetheless, these studies provide evidence that a gelatin mixture can be used to a certain extent to understand the effects of various system parameters on needle–tissue interaction dynamics.

The results presented in this study can be used in the development of needle–tissue interaction models. These models could be used to develop pre-operative plans for needle insertion procedures that require accurate needle targeting e.g. biopsy and brachytherapy.[10] Moreover, these interaction models could be used for robotically steering needles and development of surgical simulation systems.[17] Furthermore, these models would also assist in optimizing needle design.

## Funding

This work was supported by the Dutch Ministry of Economic Affairs and the Province of Overijssel, within the Pieken in de Delta (PIDON) Initiative, project MIRIAM (Minimally invasive robotics in an MRI environment).

## Conflict of interest

The author's confirm that they have no financial or personal relationships with other people or organizations that would inappropriately influence this work.

## References

1. DiMaio SP and Salcudean SE. Needle insertion modeling and simulation. *IEEE Trans Robot Automat* 2003; 19(5): 864–875.
2. Abolhassani N, Patel RV and Moallem M. Control of soft tissue deformation during robotic needle insertion. *Min Inv Therapy Allied Technol* 2006; 15(3): 165–176.
3. Lagerburg V, Moerland MA, Konings MK, et al. Development of a tapping device: a new needle insertion method for prostate brachytherapy. *Phys Med Biol* 2006; 51(4): 891–902.
4. Webster III RJ, Kim JS, Cowan NJ, et al. Nonholonomic modeling of needle steering. *Int J Robot Res* 2006; 25(5–6): 509–525.
5. Abolhassani N, Patel RV and Moallem M. Needle insertion into soft tissue: a survey. *Med Eng Phys* 2007; 29(4): 413–431.
6. Glozman D and Shoham M. Image-guided robotic flexible needle steering. *IEEE Trans Robot* 2007; 23(3): 459–467.
7. Elhawary H, Tse ZT, Rea M, et al. Robotic system for transrectal biopsy of the prostate: real-time guidance under MRI. *IEEE Eng Med Biol Mag* 2010; 29(2): 78–86.
8. Engh JA, Minhas DS, Kondziolka D, et al. Percutaneous intracerebral navigation by duty-cycled spinning of flexible bevel-tipped needles. *Neurosurgery* 2010; 67(4): 1117–1123.
9. Fütterer JJ, Misra S and Macura KJ. MRI of the prostate: potential role of robots. *Imag Med* 2010; 2(5): 583–592.

10. Misra S, Reed KB, Schafer BW, et al. Mechanics of flexible needles robotically steered through soft tissue. *Int J Robot Res* 2010; 29(13): 1640–1660.
11. Kataoka H, Washio T, Chinzei K, et al. Measurement of the tip and friction force acting on a needle during penetration. In: *Proceedings of the International Conference on Medical Image Computing and Computer-Assisted Intervention (MICCAI)* vol. 2488 of Lecture Notes in Computer Science. Berlin/Heidelberg: Springer, 2002. pp. 216–223.
12. Okamura AM, Simone C and O'Leary MD. Force modeling for needle insertion into soft tissue. *IEEE Trans Biomed Eng* 2004; 51(10): 1707–1716.
13. Podder TK, Clark DP, Fuller D, et al. Effects of velocity modulation during surgical needle insertion. In: *Proceedings of the IEEE International Conference of the Engineering in Medicine and Biology Society (EMBS)* Shanghai, China, 2005. pp. 5766–5770.
14. Abolhassani N, Patel RV and Ayazi F. Effects of different insertion methods on reducing needle deflection. In: *Proceedings of the IEEE International Conference of the Engineering in Medicine and Biology Society (EMBS)* Lyon, France, 2007. pp. 491–494.
15. Roesthuis RJ, van Veen YRJ, Jahya A, et al. Mechanics of needle-tissue interaction. In: *Proceedings of the IEEE/RSJ International Conference on Intelligent Robots and Systems (IROS)* San Francisco, USA, 2011. pp. 2557–2563.
16. Mahvash M and Dupont PE. Mechanics of dynamic needle insertion into a biological material. *IEEE Trans Biomed Eng* 2010; 57(4): 934–943.
17. Misra S, Ramesh KT and Okamura AM. Modeling of tool-tissue interactions for computer-based surgical simulation: a literature review. *Presence: Teleoperators Virtual Environ* 2008; 17(5): 463–491.